Langmuir

Article

pubs.acs.org/Langmuir

# Coarsening of Silver Nanoparticles in Polyelectrolyte Multilayers

Jingjing Wei,[†] Liming Wang,[†] Xin Zhang,[†] Xiaojing Ma,[†] Hui Wang,[‡] and Zhaohui Su*,[†]

[†]State Key Laboratory of Polymer Physics and Chemistry, Changchun Institute of Applied Chemistry, and Graduate School of Chinese Academy of Sciences, Chinese Academy of Sciences, Changchun, Jilin 130022, P. R. China

[‡]Department of Chemistry and Biochemistry, University of South Carolina, 631 Sumter Street, Columbia, South Carolina 29208, United States

Supporting Information

**ABSTRACT:** In polyelectrolyte multilayer (PEM) films assembled from poly(diallyldimethylammonium chloride) and poly(styrene sulfonate) via the layer-by-layer deposition technique, the counterions were exchanged with silver ions, which were subsequently reduced in situ to produce silver (Ag) nanoparticles. The Ag nanoparticles embedded in the PEMs were found to undergo an interesting coarsening process over time, through which smaller Ag nanoparticles coalesce into larger ones until reaching an equilibrium. The process was investigated by monitoring the localized surface plasmon resonance of the Ag nanoparticles using UV−vis extinction spectroscopy, and the spectral evolution revealed an increase in nanoparticle size with time, a trend in qualitative agreement with theoretical calculation and further confirmed by transmission electron microscopy. The kinetics of the coarsening process and the size of Ag nanoparticles at equilibrium were found to be affected by the PEM structure as well as the temperature and relative humidity the PEM was exposed to, and coalescence was identified to be the mechanism.

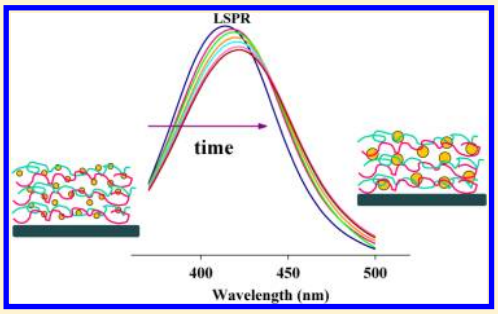


## INTRODUCTION

Noble metal nanoparticles have attracted extensive interest in recent years due to their remarkable properties and widespread applications in various fields such as catalysis, microelectronics, antibacterial agents, biosensors, and nonlinear optics.[1−3] To take full advantage of nanoparticle functions, the nanoparticles are often embedded in polymer matrices to form nanocomposite films.[4−6] Polyelectrolyte multilayer films (PEMs), assembled from oppositely charged polyelectrolytes via the layer-by-layer deposition technique, have been utilized extensively as nanoreactors and supporting matrices for the fabrication of such nanoparticle-containing nanocomposites.[7−9] For example, Bruening and co-workers assembled polyethylenimine/poly(acrylic acid) (PAA) PEMs with metal nanoparticles embedded through in situ reduction of the metal ions in the PEMs.[10,11] Rubner and co-workers introduced various metal ions into PEMs composed of weak polyelectrolytes, in particular PAA and poly(allylamine hydrochloride) (PAH), by tuning pH in the polyelectrolyte solutions, which resulted in the subsequent formation of nanoparticle-loaded PEMs upon postassembly treatment.[12] Recently, taking advantage of counterions universally present in PEMs, especially the ones constructed from strong polyelectrolytes such as poly(diallydimethylammonium chloride) (PDDA) and poly(styrene sulfonate) (PSS), we developed a general approach to PEM-based nanocomposites via ion exchange and in situ reduction process.[13,14] The composition, size, and spatial distribution of the nanoparticles synthesized in the PEM matrix can be fine-controlled,[13] and bimetallic nanoparticles with core−shell structures can be fabricated via the same strategy in PEMs as well.[15] These PEM-supported nanoparticles exhibited superior catalytic,[14] antimicrobial,[16] and photonic properties.[17]

A number of studies have revealed that polyelectrolyte chains in the layer-by-layer assembled PEMs become mobile under certain conditions and the multilayer films may undergo interesting structural changes over time. For instance, PEM films composed of PAH and PAA exhibit significant swelling/deswelling hysteresis in humid air environments.[18] Since PEMs are fabricated by alternating deposition of polyelectrolytes at solid/liquid interfaces, the salt content in polyelectrolyte solutions may have significant effects on the structural and compositional stability of the resulting PEMs.[19,20] For example, PDDA/PSS multilayers have been observed to exhibit significant mass losses when treated with salt solutions at concentrations higher than 2 M.[21] The evolution of the matrix structure is expected to have profound impact on the structures of the embedded nanoparticles as well.[22] However, in contrast to the immense efforts devoted to the controlled synthesis of PEM-supported nanoparticles, little attention has been paid to structural stability of the nanoparticles in PEM matrices.[23] Understanding how the structural changes of the PEM matrices affect the size and shape of the embedded metallic nanoparticles is of vital importance to the enhancement of our capabilities to selectively implement desired properties into metal−PEM nanocomposite materials for widespread applications due to the fact that the optical, electronic, and catalytic

Received: April 1, 2013
Revised: August 10, 2013
Published: August 14, 2013

  

properties of the metal nanoparticles are all sensitively dependent on size and shapes of the particles.[24,25] In this paper, we investigate the evolution of the size of Ag nanoparticles embedded in typical PEMs assembled from PDDA and PSS and systematically study the influence of temperature, humidity, and salt content on the kinetics of the particle size evolution.

## EXPERIMENTAL SECTION

**Materials.** PDDA (20 wt % in water, MW 200 000−350 000) and PSS (MW 70 000) were purchased from Sigma-Aldrich. Silver nitrate, sodium chloride, and sodium borohydride, all of analytical grade, were purchased from Beijing Chemical Reagents Company. All chemicals were used as received. Water (18.2 MΩ·cm) used for all the experiments was purified with a PGeneral GWA-UN4 system.

**Substrate Treatment.** Quartz slides (Jingke Optical Instrument Co., Ltd.) and glass slides (Yancheng Medical Equipment Corporation) were used as substrates. They were cleaned in a boiling piranha solution (98% $H_2SO_4$:30% $H_2O_2$, 70:30 v/v) at 80 °C for 2 h and then washed with copious amounts of water and dried under a $N_2$ stream. (*Caution: piranha solution reacts violently with organic materials and should be handled with great care.*)

**Fabrication of PEMs with Ag Nanoparticles.** PEMs (all capped with a PSS outmost layer) were assembled by sequential dipping of a substrate in PDDA (1.0 mg/mL, with NaCl present) and PSS (1.0 mg/mL, with NaCl present) aqueous solutions for 30 min each at room temperature, with water rinsing after each dipping step.[26] The cycle was repeated 5 times to yield a $(PDDA/PSS)_5$ film. The $(PDDA/PSS)_5$ films are denoted as PEM-1 and PEM-2 for the PEM assembled at a NaCl concentration of 1.0 and 1.5 M, respectively. The PEM was immersed in a $AgNO_3$ aqueous solution (0.01 M) for 10 min to exchange the $Na^+$ in the PEM for $Ag^+$, followed by rinsing with a copious amount of water. Then the film loaded with $Ag^+$ was immersed in a freshly prepared $NaBH_4$ aqueous solution (0.01 M) for 5 min to reduce $Ag^+$ into Ag nanoparticles. The composite PEMs thus prepared were transferred immediately into an incubator (constant temperature and humidity incubator LHS-100CL, Hengke Co., Ltd., Shanghai, China) maintained at a specific temperature and relative humidity. Ag nanoparticles at various stages of the coarsening process were examined by UV−vis spectroscopy.

**Characterization.** UV−vis spectra were acquired on a PerkinElmer Lambda 750 spectrometer with a 0.2 nm slit width. Two replicates were analyzed for each sample, and the average numbers are reported with error bars. Transmission electron microscopy (TEM) characterizations were carried out on a JEOL JEM-2010 microscope operating at 100 kV. A small piece of the PEM film loaded with Ag nanoparticles was peeled from the substrate in a dilute hydrofluoric acid solution and then transferred to a carbon-coated copper grid for TEM characterization.

## RESULTS AND DISCUSSION

Previous studies have demonstrated that $Ag^+$ ions can be readily introduced into PEMs via counterion exchange, and the $Ag^+$ ions can be further reduced in situ to yield Ag nanoparticles embedded in the PEMs.[13] Figure 1 shows UV−vis extinction spectra of an as-assembled PDDA/PSS PEM, the PEM with $Ag^+$ introduced, and a Ag nanoparticle−PEM composite film formed after in situ reduction for 5 min. The peak at 226 nm, which is attributed to the absorbance of the PSS, remained almost unchanged in the Ag reduction process. A new absorption peak emerged at ∼412 nm in the spectrum after in situ reduction of Ag, which corresponds to the localized surface plasmon resonance (LSPR) band of the Ag nanoparticles formed inside the PEMs. UV−vis absorbance at 412 nm was monitored as a function of the reaction time for the film, which clearly indicates that the Ag content no longer

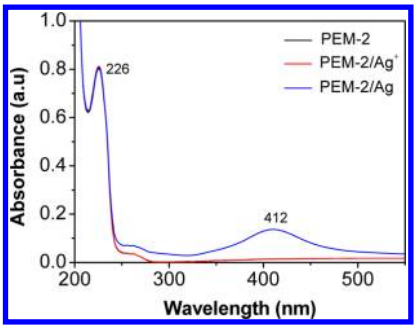


**Figure 1.** UV−vis spectra of PEM-2 film as assembled, with $Ag^+$ introduced as counterions, and after reduction of the $Ag^+$ to yield Ag nanoparticles in situ.

increased after 30 s (Supporting Information). Therefore, at 5 min reaction time, the nanoparticle formation process was complete.

Noble metal nanoparticles exhibit a unique set of optical properties that are sensitively dependent on the size, shape, and geometric arrangements of the particles. The fascinating optical characteristics of metallic nanoparticles are essentially dominated by the collective oscillations of free electrons in the metals, known as plasmons.[27−29] The plasmon resonance frequency, plasmon bandwidth, and the extinction spectral line shape altogether provide a unique spectral fingerprint for metallic nanoparticles with a specific particle composition and geometry.[30,31] A great deal of information about the physical and chemical states of the nanoparticles can be obtained by analyzing their UV−vis extinction spectra. For example, the LSPR of Ag or Au nanoparticles red-shifts as the nanoparticle size increases.[32] Therefore, UV−vis spectroscopy provides a sensitive tool for monitoring the size or shape evolution of the metallic nanoparticles.[33−35]

Figure 2 displays the evolution of the extinction spectrum of Ag nanoparticles embedded in a PEM-2 film maintained at 25

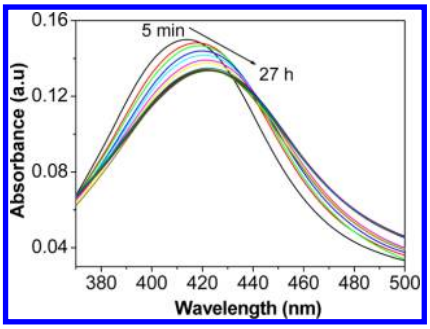


**Figure 2.** UV−vis absorption spectra of a PEM-2 film containing Ag nanoparticles acquired at varying time intervals after the Ag nanoparticles were synthesized.

°C as a function of time after fabrication. The LSPR peak of the Ag nanoparticles progressively shifted to longer wavelength from ∼412 to ∼424 nm over a time period of 27 h, indicating continuous growth in nanoparticle size over time, even in the dry PEMs.[36] It is known that larger Ag or Au nanoparticles have larger optical extinction cross sections than the smaller particles; however, the extinction peak intensity was observed to progressively decrease as the size of the embedded Ag nanoparticles increased, essentially due to the decrease in total number of Ag particles embedded in the PEMs. Since the total amount of Ag embedded in the PEMs is fixed for a given


dx.doi.org/10.1021/la401216c | Langmuir 2013, 29, 11413−11419

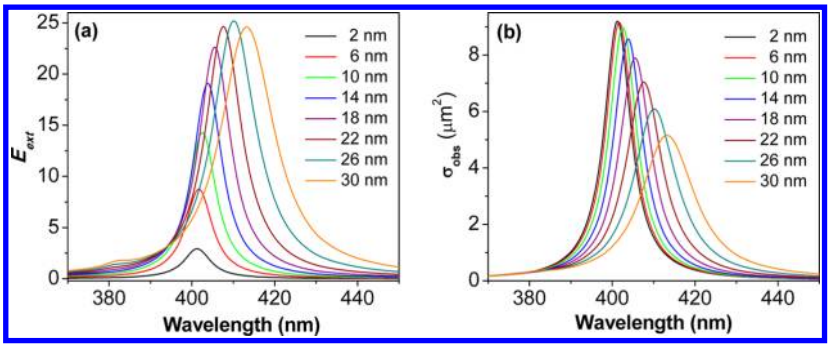


**Figure 3.** (a) Calculated extinction efficiency, $E_{ext}$, of a Ag nanosphere with varying diameter as labeled in the figure. (b) Calculated total observed extinction cross section, $\sigma_{obs}$, of Ag nanoparticles embedded in the PEM with different diameters.

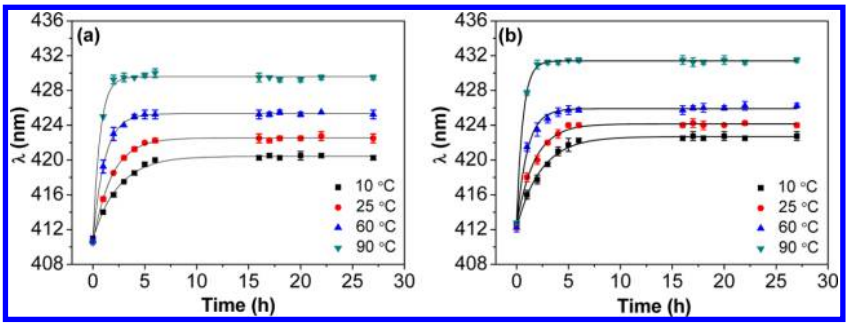


**Figure 4.** LSPR peak position $\lambda$ of PEM-1 (a) and PEM-2 (b) loaded with Ag nanoparticles as a function of time obtained at different temperature and 30% relative humidity. The data are fitted with exponential decay functions represented by the corresponding solid lines.

nanocomposite sample, the total number of Ag nanoparticles would decrease when the smaller particles undergo a coarsening process to form bigger particles.

To gain further insights into the extinction spectral evolution of the embedded Ag nanoparticles, we theoretically calculated scattering, absorption, and extinction spectra of the nanoparticles using the Mie scattering theory.[37] In these calculations, we assumed perfectly spherical particle geometry and a homogeneous dielectric medium surrounding the nanoparticles with a dielectric constant of 2.25. The wavelength-dependent empirical dielectric functions of bulk Ag[38] were used. The calculated extinction was expressed as optical extinction (scattering + absorption) efficiency ($E_{ext}$), which was the ratio of the total energy scattered and absorbed by the particle to the energy incident on the physical cross section of the particle. As shown in Figure 3a, the extinction peak of a Ag nanoparticle progressively red-shifted, accompanied by an increase in the extinction efficiency, as the particle became bigger. The extinction cross section of a Ag nanoparticle is dramatically amplified as the particle size increases due to the increase in both the physical cross section and the extinction efficiency of the particle. If we assume there are initially $10^6$ Ag nanoparticles (2 nm diameter) in the PEM film and the total amount of metallic Ag embedded in the PEM is fixed at this amount during the nanoparticle growth, the total observed extinction cross section ($\sigma_{obs}$) can be calculated using the equation

$$\sigma_{obs} = \pi E_{ext}/r \ (\mu m^2)$$

where $r$ is the radius of the Ag nanospheres. As shown in Figure 3b, $\sigma_{obs}$ decreased as the particle size increased simply due to the decrease in total number of particles embedded in the PEM film. The calculated results, both the LSPR shift and the $\sigma_{obs}$ evolution upon changes of the particle size, are in qualitative agreement with the experimental observations. The experimental LSPR bands turned out to be broader than the calculated ones largely due to the size distributions and structural nonideality of the experimentally fabricated particles. The structural heterogeneity inside the PEM films may also provide an inhomogeneous local dielectric environment surrounding each Ag nanoparticle. The effects of surface electron scattering[39] and plasmon quantum confinement,[40] which become increasingly significant when Ag nanoparticles are in the sub-10 nm size regime, may further introduce modifications to the Ag dielectric functions. Gaining more detailed and quantitative insights into the relationship between particle geometry and LSPR properties of Ag nanoparticles requires correlated single-particle spectroscopic measurements and electrodynamic simulations, which were not further pursued in this work.

A classical mechanism for nanoparticle growth in solutions is through monomer addition to the nuclei formed in a preceding nucleation period.[41] Whereas, recent studies have shown that clusters composed of several atoms, such as $Ag_{13}$ or $Au_{13}$ clusters, play an important role as elementary species that guide the growth of Ag or Au nanoparticles,[41,42] and alternative pathways involved in the size evolution and growth of metal nanoparticles can also be found in other reports.[43,44] However, all these proposed mechanisms are for nanoparticle growth in the solution phase where intermediate species are present to facilitate mass transfer from one (smaller) particle to another (bigger). Knowledge about the growth of nanoparticles embedded in solid state matrices has been very limited so far, yet a better understanding of the growth mechanisms of metal nanoparticles in PEMs is crucial to further manipulation of the properties of the nanocomposite films.

We systematically studied the coarsening process of the Ag nanoparticles embedded in the PEM films at various temperatures and relative humidity. The LSPR peak wavelength ($\lambda$)


dx.doi.org/10.1021/la401216c | *Langmuir* 2013, 29, 11413−11419

was used to represent average size of the nanoparticles, and the $\lambda$ as a function of incubation time at different temperatures is plotted in Figure 4. It can be seen that a spectral red-shift over time occurred in each sample. All samples prepared under the same conditions exhibited the same initial extinction peak ($\lambda_0$) after fresh preparation but showed various final extinction peak wavelengths ($\lambda_\infty$) after staying at different temperatures for several hours. The plots clearly show that the size of the Ag nanoparticles increased quickly in the initial stage and then approached a plateau value with time until equilibrium was reached, and temperature has significant effects on the kinetics of the nanoparticle growth.

To quantitatively analyze the data for Ag nanoparticles coarsening under different conditions, the peak position data were fitted to the following single exponential decay function

$$\frac{\lambda_\infty - \lambda}{\lambda_\infty - \lambda_0} = e^{-kt}$$

where $k$ is a constant for $\lambda$ evolution with time and thus can represent the particle growth rate constant. The experimental data were fitted through a least-squares curve fitting process using this first-order kinetics equation.

The curve fitting results for Figure 4 are summarized in Table 1. We found that the kinetics of the particle coarsening process and the final particle size at equilibrium were mainly determined by three factors: ambient temperature, air relative humidity, and salt concentration in the depositing solutions for the PEMs.

**Table 1. Summary of the Curve-Fitting Results for Different Temperatures**

| | | temperature (°C) | | | |
|---|---|---|---|---|---|
| PEM | | 10 | 25 | 60 | 90 |
| PEM-1 | $\lambda_0$ (nm) | 410.5 | 410.5 | 410.5 | 410.5 |
| | $\lambda_\infty$ (nm) | 420.1 | 422.5 | 425.0 | 429.5 |
| | $k$ ($h^{-1}$) | 0.39 | 0.56 | 0.88 | 1.50 |
| PEM-2 | $\lambda_0$ (nm) | 412.5 | 412.5 | 412.5 | 412.5 |
| | $\lambda_\infty$ (nm) | 422.7 | 424.0 | 425.9 | 431.4 |
| | $k$ ($h^{-1}$) | 0.43 | 0.58 | 0.98 | 1.70 |

It is obvious from both the plots in Figure 4 and the numbers in Table 1 that the $\lambda_\infty$ increases with temperature, indicating the increase of the final size of the Ag nanoparticles with temperature. This was further confirmed by TEM measurements as shown in Figure 5. In PEM-2 the average particle radius grew from 2.1 nm into 4.1, 8.1, 13.4, and 25.6 nm after equilibration at 10, 25, 60, and 90 °C, respectively. While the formation of small particles is kinetically favored, the coarsening process is essentially driven by thermodynamics. During the reduction process it is easier to nucleate so as to form many small particles in the early stage. However, smaller particles have higher specific surface areas than large particles, and the total surface energy would be much higher if only very small Ag nanoparticles were formed in the PEMs compared with large Ag nanoparticles. Thus, the coarsening of small particles into large ones can distinctly lower the surface energy of the system, making the larger particles more stable. There are two possible mechanisms for the increase in average size of the Ag nanoparticles: coalescence of the particles and Ostwald ripening.[45] Ag does not spontaneously dissolve in PEM or water, and there is no plausible intermediate species in the system (Supporting Information) to assist the dissolution and transport of Ag from one particle to another. Therefore, we conclude that the Ag nanoparticles in the PEM grow via coalescence. In fact, in Figure 5d, some big particles appear to be aggregates of smaller ones, providing direct evidence for this mechanism.

It is interesting to find that step heating leads to similar result as direct heating. A PEM-2 film containing Ag particles was first maintained at 10 °C until the average particle size (characterized by $\lambda$) reached a plateau value, and then the temperature was further increased to 90 °C, under which the particles continued to grow and eventually reached a new plateau value. As seen in Figure 6, $\lambda_\infty$, hence the particle size at equilibrium, obtained through this stepwise heating process was the same as that for the particles maintained at 90 °C all the way through. The fact that the equilibrium particle size value is a function of temperature while independent of the path leading to the final temperature further suggests that the final particle size is determined by thermodynamics.

From Figure 4 it is also clear that the time needed for the particles to reach their equilibrium sizes is shorter at higher temperature. Generally, temperature can significantly affect the rate of a chemical/physical process, and the influence of temperature on a chemical reaction may be quantitatively described by the Arrhenius equation. For a first-order reaction with a rate constant $k$, a plot of ln $k$ versus $1/T$ should give a straight line, the slope of which is related to the activation energy of the reaction. In our case, $k$ determined by curve-fitting discussed above represents the rate constant for the particle size increase. As seen in Table 1, the apparent rate constant has strong dependence on temperature. Figure 7 plots ln $k$ versus $1/T$, and a linear relationship is observed, which indicates that Arrhenius equation is a simple but still remarkably accurate formula for describing the temperature dependence of the particle growth process in the PEM matrix.

Salt in polyelectrolyte solutions is known to exhibit a strong influence on the structure and properties of the layer-by-layer assembled PEMs[20] and thus is expected to impact the particle coarsening process occurring in the PEM matrix. As shown in Figure 4 and Table 1, at the same temperature, Ag nanoparticles embedded in PEM-2 (assembled at a NaCl concentration of 1.5 M) were bigger initially (a higher $\lambda_0$), grew faster (a greater $k$), and reached a larger equilibrium size (a higher $\lambda_\infty$) than their counterparts in PEM-1 (assembled at a NaCl concentration of 1.0 M). In Figure 7, the slope of the ln $k$ versus $1/T$ plot was smaller for the particles in PEM-2 than in PEM-1. The empirical activation energy derived from the slope was 14.4 and 13.3 kJ/mol for particle coalescence in PEM-1 and PEM-2, respectively. In a PEM assembled at a higher salt concentration, more of the polyelectrolyte units are compensated by small counterions. The higher counterion content results in bigger Ag nanoparticles as prepared,[13] and the fewer polyelectrolyte repeat unit pairs, the ionic cross-links, lead to more mobile polyelectrolyte chain segments in the PEM,[46] which should facilitate the mass transport in the PEM. In addition, the presence of more hydrophilic counterions may increase the water content in the PEM, which can facilitate the mass transport as well (see below). Therefore, in a PEM assembled at a higher salt concentration the activation energy for the particle coalescence is lower, and the nanoparticle growth is faster.

Another factor that can affect PEMs is relative humidity.[47] It was shown that a PDDA/PSS PEM can contain ~26% water at

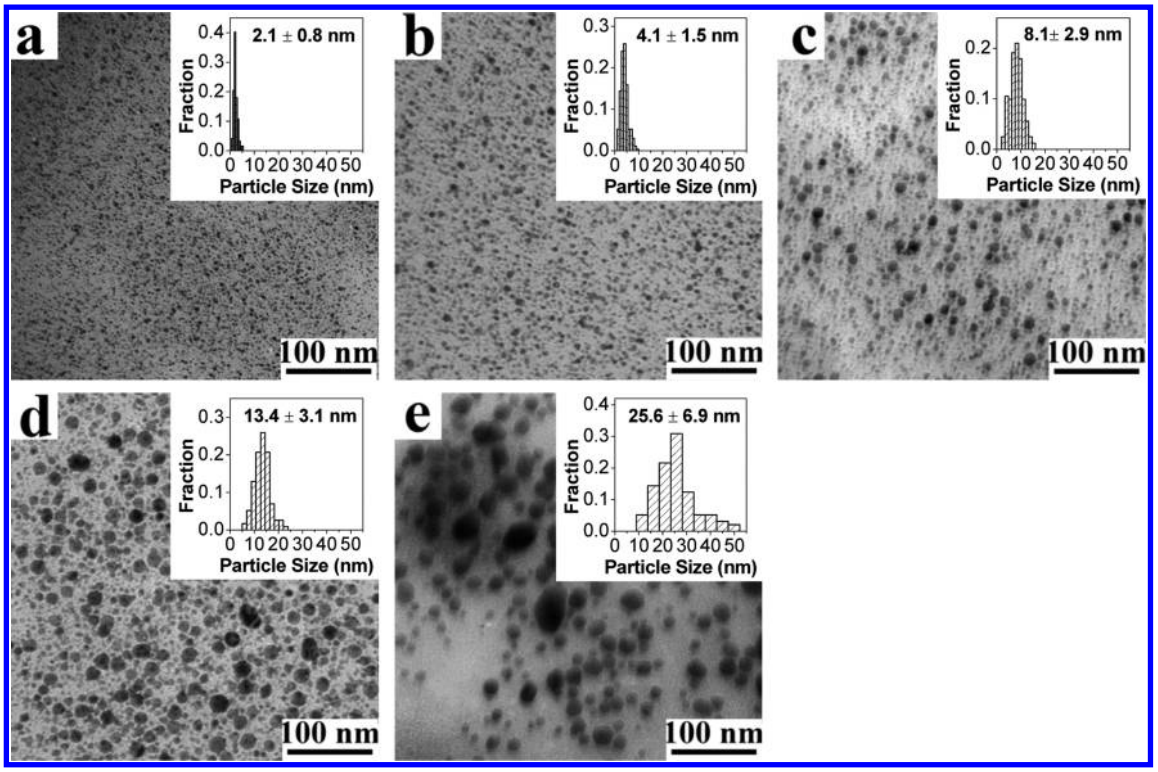


**Figure 5.** TEM images of Ag nanoparticles embedded in PEM-2 as prepared (a) and after equilibration at 10 (b), 25 (c), 60 (d), and 90 °C (e). The insets are the corresponding particle size histograms.

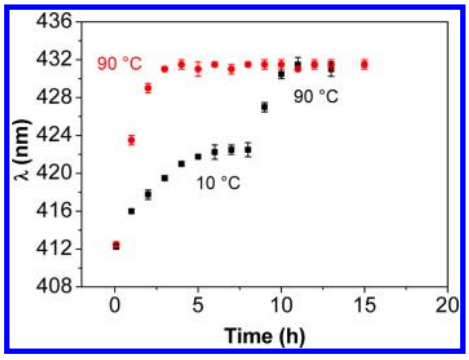


**Figure 6.** LSPR peak position $\lambda$ as a function of time for Ag nanoparticles embedded in PEM-2 incubated using different temperature profiles.

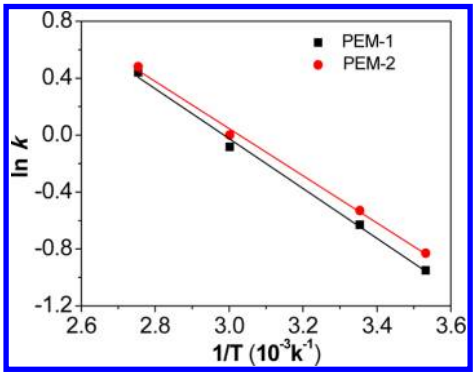


**Figure 7.** Plot of ln $k$ as a function of temperature for Ag nanoparticle growth in PEM-1 (black square) and PEM-2 (red circle).

100% relative humidity.[48] Figure 8 compares Ag particle growth at 0%, 30%, and 90% relative humidity, and the curve-fitting results are summarized in Table 2. It can be seen that the final size of Ag nanoparticles at equilibrium and the particle growth rate both increased with relative humidity. This is because water acts as a plasticizer for the PEM to increase the mobility of the polyelectrolyte segments in the matrix, resulting in faster mass transport that facilitates the particle growth process.

## CONCLUSION

The polymer chains inside the PEMs are mobile rather than being fixed, and the PEMs may undergo structural changes under suitable conditions. The structural changes of the PEM matrices may give rise to interesting size and shape evolution of the nanoparticles embedded in the PEMs. Here, we have observed that Ag nanoparticles embedded in PDDA/PSS PEMs undergo an interesting coalescence process upon incubation under different ambient conditions. The Ag nanoparticles tend to grow into larger ones until equilibrium is reached and the coalescence process follows first-order kinetics. We have investigated three factors that significantly affect the coarsening processes: the temperature, relative humidity, and PEM structure as mediated by the salt concentration in the depositing solutions. Both the particle growth rate and the final particle size at equilibrium were found to increase with the temperature, relative humidity, and salt concentration. Our results demonstrate the coalescence of nanoparticles in PEM matrices and correlate the kinetics with chain dynamics in the PEM. On the basis of these findings, it is also conceivable that the nanoparticle coalescence process would significantly slow down or freeze when the polyelectrolyte chain motion is severely restricted, such as at much lower temperatures or in more glassy PEMs. These factors need to be considered when nanoparticle size control is important for designated applications.


dx.doi.org/10.1021/la401216c | Langmuir 2013, 29, 11413−11419

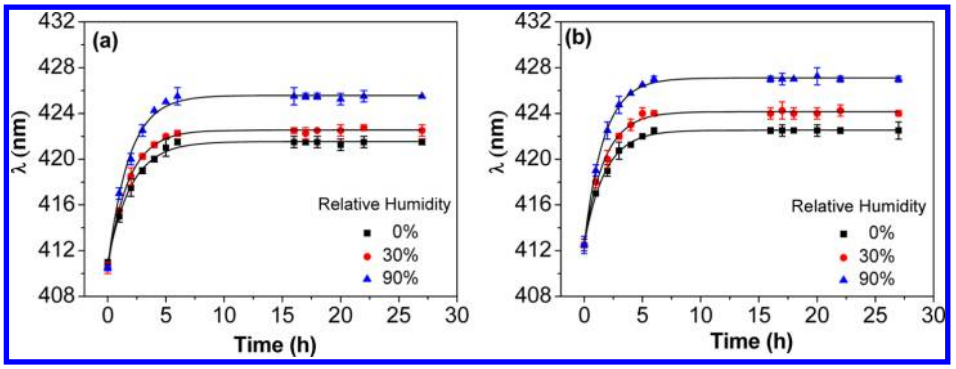


**Figure 8.** LSPR peak position $\lambda$ of PEM-1 (a) and PEM-2 (b) loaded with Ag nanoparticles as a function of time obtained at different relative humidity at 25 °C. The data are fitted with exponential decay functions represented by the corresponding solid lines.

**Table 2. Summary of the Curve-Fitting Results for Different Relative Humidity**

| | | relative humidity | | |
|---|---|---|---|---|
| PEM | | 0% | 30% | 90% |
| PEM-1 | $\lambda_0$ (nm) | 410.5 | 410.5 | 410.5 |
| | $\lambda_\infty$ (nm) | 421.5 | 422.5 | 425.5 |
| | $k$ ($h^{-1}$) | 0.54 | 0.56 | 0.59 |
| PEM-2 | $\lambda_0$ (nm) | 412.5 | 412.5 | 412.5 |
| | $\lambda_\infty$ (nm) | 422.5 | 424.0 | 427.0 |
| | $k$ ($h^{-1}$) | 0.56 | 0.58 | 0.60 |

## ■ ASSOCIATED CONTENT

### Supporting Information

UV−vis data showing in situ reduction kinetics and particle growth kinetics in the absence of $Cl^-$, AFM images, and TEM images for PEM-1 containing Ag nanoparticles. This material is available free of charge via the Internet at http://pubs.acs.org.

## ■ AUTHOR INFORMATION

### Corresponding Author

*E-mail: zhsu@ciac.ac.cn.

### Notes

The authors declare no competing financial interest.

## ■ ACKNOWLEDGMENTS

This work is supported by National Natural Science Foundation of China (21174145). Z.S. thanks the NSFC Fund for Creative Research Groups (50921062) for support. H.W. acknowledges the support by NSF CAREER Award (DMR-1253231).

## ■ REFERENCES

(1) Fendler, J. H. *Nanoparticles and Nanostructured Films*; Wiley-VCH: Weinheim, 2008; pp 263−274.

(2) Nie, Z. H.; Petukhova, A.; Kumacheva, E. Properties and Emerging Applications of Self-assembled Structures Made from Inorganic Nanoparticles. *Nat. Nanotechnol.* **2010**, *5*, 15−25.

(3) Dykman, L.; Khlebtsov, N. Gold Nanoparticles in Biomedical Applications: Recent Advances and Perspectives. *Chem. Soc. Rev.* **2011**, *41*, 2256−2282.

(4) Shenhar, R.; Norsten, T. B.; Rotello, V. M. Polymer-Mediated Nanoparticle Assembly: Structural Control and Applications. *Adv. Mater.* **2005**, *17*, 657−669.

(5) Russell, T. P.; Balazs, A. C.; Emrick, T. Nanoparticle Polymer Composites: Where Two Small Worlds Meet. *Science* **2006**, *314*, 1107−1110.

(6) Decher, G.; Eckle, M.; Schmitt, J.; Struth, B. Layer-by-Layer Assembled Multicomposite Films. *Curr. Opin. Colloid Interface Sci.* **1998**, *3*, 32−39.

(7) Decher, G. Fuzzy Nanoassemblies: Toward Layered Polymeric Multicomposites. *Science* **1997**, *277*, 1232−1237.

(8) Ariga, K.; Hill, J. P.; Ji, Q. M. Layer-by-Layer Assembly As a Versatile Bottom-up Nanofabrication Technique for Exploratory Research and Realistic Application. *Phys. Chem. Chem. Phys.* **2007**, *9*, 2319−2340.

(9) (a) Gong, X.; Han, L.; Yue, Y. N.; Gao, J. R.; Gao, C. Y. Influence of Assembly pH on Compression and Ag Nanoparticle Synthesis of Polyelectrolyte Multilayers. *J. Colloid Interface Sci.* **2011**, *355*, 368−373. (b) Skirtach, A. G.; Antipov, A. A.; Shchukin, D. G.; Sukhorukov, G. B. Remote Activation of Capsules Containing Ag Nanoparticles and IR Dye by Laser Light. *Langmuir* **2004**, *20*, 6988−6992.

(10) Dai, J. H.; Bruening, M. L. Catalytic Nanoparticles Formed by Reduction of Metal Ions in Multilayered Polyelectrolyte Films. *Nano Lett.* **2002**, *2*, 497−501.

(11) Kidambi, S.; Dai, J. H.; Li, J.; Bruening, M. L. Selective Hydrogenation by Pd Nanoparticles Embedded in Polyelectrolyte Multilayers. *J. Am. Chem. Soc.* **2004**, *126*, 2658−2659.

(12) Wang, T. C.; Cohen, R. E.; Rubner, M. F. Metallodielectric Photonic Structures Based on Polyelectrolyte Multilayers. *Adv. Mater.* **2002**, *14*, 1534−1537.

(13) Zan, X. J.; Su, Z. H. Incorporation of Nanoparticles Into Polyelectrolyte Multilayers via Counterion Exchange and In Situ Reduction. *Langmuir* **2009**, *25*, 12355−12360.

(14) Zan, X. J.; Su, Z. H. Counterions in Polyelectrolyte Multilayers: a Vehicle for Introducing Functionalities. *Thin Solid Films* **2009**, *518*, 116−119.

(15) Zhang, X.; Su, Z. H. Polyelectrolyte-Multilayer-Supported Au@Ag Core-Shell Nanoparticles with High Catalytic Activity. *Adv. Mater.* **2012**, *24*, 4574−4577.

(16) Cohen, R. E.; Lee, D.; Rubner, M. F. Antibacterial Properties of Ag Nanoparticle Loaded Multilayers and Formation of Magnetically Directed Antibacterial Microparticles. *Langmuir* **2005**, *21*, 9651−9659.

(17) Hiller, J.; Mendelsohn, J. D.; Rubner, M. F. Reversibly Erasable Nanoporous Anti-Reflection Coatings from Polyelectrolyte Multilayers. *Nat. Mater.* **2002**, *1*, 59−63.

(18) Nolte, A. J.; Secrist, K. E. Humidity Swelling/Deswelling Hysteresis in a Polyelectrolyte Multilayer Film. *Macromolecules* **2011**, *44*, 2859−2865.

(19) Steitz, R.; Jaeger, W.; von Klitzing, R. Influence of Charge Density and Ionic Strength on the Multilayer Formation of Strong Polyelectrolytes. *Langmuir* **2001**, *17*, 4471−4474.

(20) Dubas, S. T.; Schlenoff, J. B. Factors Controlling the Growth of Polyelectrolyte Multilayers. *Macromolecules* **1999**, *32*, 8153−8160.

(21) Han, L. L.; Mao, Z. W.; Wuliyasu, H.; Wu, J. D.; Gong, X.; Yang, Y. G.; Gao, C. Y. Modulating the Structure and Properties of Poly(sodium 4-styrenesulfonate)/Poly(diallyldimethylammonium chloride) Multilayers with Concentrated Salt Solutions. *Langmuir* **2012**, *28*, 193−199.

(22) Lee, S. J.; An, H. H.; Han, W. B.; Kim, H. S.; Yoon, C. S. Effect of Temperature and Humidity on Coarsening Behavior of Au Nanoparticles Embedded in Liquid Crystalline Lipid Membrane. *Langmuir* **2012**, *28*, 10980−10987.
(23) Meristoudi, A.; Pispas, S. Polymer Mediated Formation of Corona-Embedded Gold Nanoparticles in Block Polyelectrolyte Micelles. *Polymer* **2009**, *50*, 2743−2751.
(24) Daniel, M. C.; Astruc, D. Gold Nanoparticles: Assembly, Supramolecular Chemistry, Quantum-Size-Related Properties, and Applications toward Biology, Catalysis, and Nanotechnology. *Chem. Rev.* **2004**, *104*, 293−346.
(25) Xia, Y. N.; Rycenga, M.; Cobley, C. M.; Zeng, J.; Li, W. Y.; Moran, C. H.; Zhang, Q.; Qin, D. Controlling the Synthesis and Assembly of Silver Nanostructures for Plasmonic Applications. *Chem. Rev.* **2011**, *111*, 3669−3712.
(26) Zhang, X.; Chu, C. C.; Huang, K. H.; Su, Z. H. Preparation of Au@Pt Core-Shell Nanoparticles Using Polyelectrolyte Multilayers as Nanoreactors. *Chin. J. Appl. Chem.* **2012**, *29*, 1433−1437.
(27) Mulvaney, P. Surface Plasmon Spectroscopy of Nanosized Metal Particles. *Langmuir* **1996**, *12*, 788−800.
(28) Schatz, G. C.; Sherry, L. J.; Jin, R. C.; Mirkin, C. A.; Van Duyne, R. P. Localized Surface Plasmon Resonance Spectroscopy of Single Silver Triangular Nanoprisms. *Nano Lett.* **2006**, *6*, 2060−2065.
(29) El-Sayad, M. A.; Jain, P. K.; Huang, X.; El-Sayed, I. H. Review of Some Interesting Surface Plasmon Resonance-enhanced Properties of Noble Metal Nanoparticles and Their Applications to Biosystems. *Plasmonics* **2007**, *2*, 107−118.
(30) Yavuz, M. S.; Cheng, Y. Y.; Chen, J. Y.; Cobley, C. M.; Zhang, Q.; Rycenga, M.; Xie, J. W.; Kim, C.; Song, K. H.; Schwartz, A. G.; Wang, L. H. V.; Xia, Y. N. Gold Nanocages Covered by Smart Polymers for Controlled Release with Near-infrared Light. *Nat. Mater.* **2009**, *8*, 935−939.
(31) Wiley, B.; Sun, Y. G.; Xia, Y. N. Synthesis of Silver Nanostructures with Controlled Shapes and Properties. *Acc. Chem. Res.* **2007**, *40*, 1067−1076.
(32) Lee, K. C.; Lin, S. J.; Lin, C. H.; Tsai, C. S.; Lu, Y. J. Size Effect of Ag Nanoparticles on Surface Plasmon Resonance. *Surf. Coat. Technol.* **2008**, *202*, 5339−5342.
(33) Silva, A. M. B.; de Araujo, C. B.; Santos-Silva, S.; Galembeck, A. Silver Nanoparticle in Situ Growth within Crosslinked Poly(ester-co-styrene) Induced by UV Irradiation: Aggregation Control with Exposure Time. *J. Phys. Chem. Solids* **2007**, *68*, 729−733.
(34) Liu, K.; Nie, Z. H.; Zhao, N. N.; Li, W.; Rubinstein, M.; Kumacheva, E. Step-Growth Polymerization of Inorganic Nanoparticles. *Science* **2010**, *329*, 197−200.
(35) Mock, J. J.; Barbic, M.; Smith, D. R.; Schultz, D. A.; Schultz, S. Shape Effects in Plasmon Resonance of Individual Colloidal Silver Nanoparticles. *J. Chem. Phys.* **2002**, *116*, 6755−6759.
(36) Link, S.; El-Sayed, M. A. Spectral Properties and Relaxation Dynamics of Surface Plasmon Electronic Oscillations in Gold and Silver Nanodots and Nanorods. *J. Phys. Chem. B* **1999**, *103*, 8410−8426.
(37) Mie, G. Beiträge zur Optik trüber Medien, Speziell Kolloidaler Metallösungen. *Ann. Phys,* **1908**, *330*, 377−445.
(38) Johnson, P. B.; Christy, R. W. Optical Constants of the Noble Metals. *Phys. Rev. B* **1972**, *6*, 4370−4379.
(39) Westcott, S. L.; Jackson, J. B.; Radloff, C.; Halas, N. J. Relative Contributions to the Plasmon Line Shape of Metal Nanoshells. *Phys. Rev. B* **2002**, *66*, 155431−155435.
(40) Scholl, J. A.; Koh, A. L.; Dionne, J. A. Quantum Plasmon Resonances of Individual Metallic Nanoparticles. *Nature* **2012**, *483*, 421−U468.
(41) Takesue, M.; Tomura, T.; Yamada, M.; Hata, K.; Kuwamoto, S.; Yonezawa, T. Size of Elementary Clusters and Process Period in Silver Nanoparticle Formation. *J. Am. Chem. Soc.* **2011**, *133*, 14164−14167.
(42) Schmid, G. The Relevance of Shape and Size of Au-55 Clusters. *Chem. Soc. Rev.* **2008**, *37*, 1909−1930.
(43) Kolb, M.; Botet, R.; Jullien, R. Scaling of Kinetically Growing Clusters. *Phys. Rev. Lett.* **1983**, *51*, 1123−1126.
(44) Silvert, P. Y.; HerreraUrbina, R.; TekaiaElhsissen, K. Preparation of Colloidal Silver Dispersions by the Polyol Process 0.2. Mechanism of Particle Formation. *J. Mater. Chem.* **1997**, *7*, 293−299.
(45) Brailsford, A.; Wynblatt, P. The Dependence of Ostwald Ripening Kinetics on Particle Volume Fraction. *Acta Metall.* **1979**, *27*, 489−497.
(46) Shamoun, R. F.; Andreas, R.; Schlenoff, J. B. Extruded Saloplastic Polyelectrolyte Complexes. *Adv. Funct. Mater.* **2012**, *22*, 1923−1931.
(47) Gao, C. Y.; Wang, B.; Feng, J.; Shen, J. C. Irreversible Compression of Polyelectrolyte Multilayers. *Macromolecules* **2004**, *37*, 8836−8839.
(48) Farhat, T.; Yassin, G.; Dubas, S. T.; Schlenoff, J. B. Water and Ion Pairing in Polyelectrolyte Multilayers. *Langmuir* **1999**, *15*, 6621−6623.